A Fully Autonomous Ultra-low Power Hybrid RF/Photovoltaic Energy Harvesting System with -25 dBm Sensitivity

Jo Bito†, Jimmy G. Hester and Manos M. Tentzeris
School of Electrical and Computer Engineering
Georgia Institute of Technology
Atlanta, GA 30308 USA
†jbito3@gatech.edu

***Abstract*—This study discusses the design process of a novel fully autonomous ultra-low power hybrid RF/photovoltaic energy harvesting system. As a result of the simulated and measured relationship between the output voltage of the rectifier and the load resistance value, the optimal rectifier topology and the charge tank capacitor value are analytically determined. One proof-of-concept designed and fabricated rectifier prototype exhibits the peak and average RF-dc conversion efficiency of 24.0% and 17.6% while charging a charge tank capacitor with -20 dBm of RF power. Similarly, a photovoltaic powered dc-dc converter circuit which requires the minimum power of 59 nW and operates under the low light irradiation of 3 lx ($440\ nW/cm^2$) is designed and features the capability of successfully charging the output capacitor up to more than 2.4 V with the output power of 643 nW from -20 dBm of RF input power. The proposed system can generate net positive output power from -25.0 dBm of RF input power.**

***Index Terms*—Energy harvesting, RF, IoT, hybrid system, solar, organic, photovoltaic, inkjet printing, sensor, power management**

I. Introduction

These days, the desire for a smart society that utilizes technologies such as large-scale sensor networks and the Internet of Things (IoT) is strengthening. One of the most pressing issues is the lack of sustainable power supplies that could enable the autonomous operation of these sensors and devices (mote). Conventional autonomous devices heavily rely on primary batteries which need replacement after a while, and the cost of replacing batteries increases significantly as the number of sensor devices increases. To avoid this maintenance cost issue and achieve completely self-sustainable low-cost ubiquitous systems for the IoT and smart cities, research communities have devoted a considerable interest in ambient energy harvesting technologies. Among the ambient energy sources, RF energy is a highly attractive energy source because of its almost ubiquitous availability, especially in urban areas, and the low cost and size of transducers [1]. However, compared to the energy density of other energy sources, that of RF energy is typically very low, so RF energy harvesters cannot directly drive devices that require relatively high power and voltage such as micro-controllers, especially from a cold-start condition. Since low energy density also causes low RF-dc conversion efficiency, RF energy harvesting is even more challenging to be practically exploited. To overcome these challenges, Gudan et al. have reported an ultra-low required power energy harvesting and charging system utilizing long-term duty cycling and self-resonance type Armstrong oscillator [2] minimizing the required power and voltage for the effective operation of autonomous systems. However, the dc-dc conversion efficiency is still relatively low because of inevitable loss associated with the use of Armstrong oscillators. The bottleneck to use more efficient oscillators for the dc-dc converters is the operation voltage of the oscillator ICs, which is typically more than $1\,\mathrm{V}$ that RF-dc converter circuits cannot generate with RF input power below $-20\,\mathrm{dBm}$, which is a typical value for ambient RF energy harvesting, especially at operation frequencies more than $1\,\mathrm{GHz}$. However, this challenge can be easily addressed by combining other ambient energy sources such as photovoltaic (PV) even under room light or darkroom irradiation conditions. Several works have reported the use of hybrid RF/solar energy harvesters in a system. As an example, Niotaki et al. have reported on a hybrid RF/solar energy harvester, which can significantly increase the total available power in a system [3]. However, for ambient RF energy harvesting applications, a typical off-the-shelf solar cell can easily generate more than -10 dBm of dc power even under relatively low room light irradiation condition ($100\,\mu\mathrm{W}\cdot\mathrm{cm}^{-2}$) and dominates the total dc power generation in the hybrid RF/solar energy harvesting system [3]. Although, with even lower irradiance levels such as the ones found in darkroom (ca. below $10\,\mu\mathrm{W}\cdot\mathrm{cm}^{-2}$), the energy conversion efficiency of a photovoltaic device becomes limited by increased power losses that arise as the value of the devices shunt resistance becomes comparable to that of the characteristic resistance of the cell. The available dc power from a solar cell linearly decreases with respect to the light intensity. On the other hand, open voltage of a solar cell decreases linearly with respect to the logarithmic scale reduction of the light intensity [4], [5]. These imply that a solar cell can provide sufficiently high voltage while output power is very limited under a low-light level operation. Therefore, a solar cell is better to be used as a voltage source to operate a extremely low-power-required power management circuit to convert the energy from an RF-dc conversion circuit, which is a main energy source in the system, into high voltage usable form increasing the RF sensitivity of the system. Also, both RF and solar energy harvesters as well as fundamental circuit components such as antenna are well compatible with inkjet printing technology, which is the key enabler of low-cost IoT device fabrication [6]–[8].

978-1-5090-4585-3/17/$31.00 ©2017 IEEE

In this paper, an ultra-low power hybrid RF solar energy harvesting system utilizing Texas Instruments TPL5100 nano-timer and Silicon Labs TS3001 oscillator ICs. The PV-powered timer, which consumes power below $50\,\mathrm{nW}$, generates short duration pulse signals with operation frequency below $0.1\,\mathrm{Hz}$ to trigger the operation of a relatively high-power and frequency (1 to $5\,\mu\mathrm{W}$ at 5 to $90\,\mathrm{kHz}$ oscillation frequency) oscillator to minimize the power consumption of entire system. This low required energy allows the operation of the system even under extremely low light irradiation condition without having the issue of cold start. Fig. 1 depicts the block diagram of the system. Expected RF input power level is $-20\,\mathrm{dBm}$ at $2.4\,\mathrm{GHz}$ ISM band.

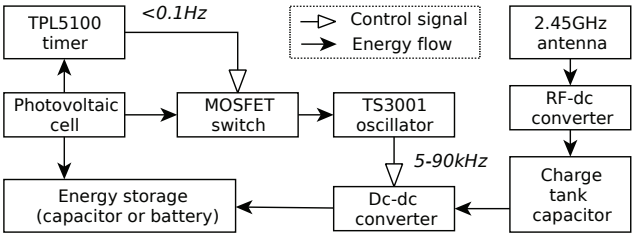

Fig. 1. Block diagram of the proposed hybrid RF/PV powered energy harvesting system.

II. Selection of Rectifier Topology and Charge Tank Capacitor Value

There are several rectifier topologies available which exhibit different maximum RF-dc conversion efficiency, optimum load resistance, and open voltage values. This research compares the performance of a series rectifier, a one-stage and a two-stage voltage multiplier to select the optimal RF-dc conversion circuit topology, which exhibits the highest RF-dc conversion efficiency, and charge tank capacitor value for long-term duty cycling through simulation and analytical estimation. In the proof-of-concept simulation with Keysight Advanced Design System (ADS), Avago HSMS285 Schottky diode and $0.5\,\mathrm{mm}$ thick Rogers RO4003 substrate were utilized. For impedance matching, a radial stub with optimized length (S_L), distance from the anode of the diode (S_P), and the stub angle (S_A) was utilized. The microstrip line width and the width of stub input line is $1.15\,\mathrm{mm}$ making the characteristic impedance of the lines to be $50\,\Omega$. Table I summarizes the results of simulation. As a clear trend, the peak RF-dc conversion efficiency decreases and the open voltage increases as the number of diodes increases. To maximize the energy available in a capacitor within a specific time period, the transient behavior of the charging of the capacitor needs to be simulated. However, since the RF-dc conversion circuit is a load resistance dependent power supply, the charging of the capacitor, which changes its equivalent impedance value continuously while charging, cannot be simply modeled with well known capacitor charging models with a perfect voltage or current source. Similarly, in ADS transient simulation, from Shannon's sampling theorem, the time step needs to be at least $0.2\,\mathrm{ns}$ to express $2.5\,\mathrm{GHz}$ signals making practically impossible to simulate the behavior of the capacitor for a time period more than $1\,\mathrm{s}$ because of the simulation time and the memory requirement, especially with a varied charge tank capacitance value. On the other hand, the steady state voltage at each given load resistance value can be immediately simulated from harmonic balance simulation in ADS. From Ohm's law and the definition of current in a capacitor, the capacitor impedance variation over the time can be expressed as shown in equation (1) where $V(t)$, $Z(t)$, and C are the output voltage, load resistance, and charge tank capacitance, respectively. From the relationship between the output voltage and the load resistance, the slope of voltage for each given load resistance ($\frac{dV}{dZ}$) can be easily calculated. If the output voltage, load resistance and the slope of the voltage at $t = 0$ are given as initial conditions, the capacitor impedance and voltage variation over the time can be numerically calculated utilizing equation (1). Once the output voltage at each time step is determined, the energy stored in the capacitor ($E = \frac{1}{2}CV^2$) can be also easily calculated. Practically, the output voltage of the rectifier cannot be measured continuously changing load resistance, and the relationship is typically calculated at discrete data points. Therefore, without loss of generality, the measured output voltage and its relationship with the load is approximately expressed as closed form equations shown as equation (2) where p_1, p_2, and q_1 are arbitrary constant terms derived through MATLAB polynomial fitting function. Fig. 2 shows the average RF-dc conversion efficiency ($\eta_{avg} = \frac{E}{t_p}$) for every rectifier topology with varied capacitance value at selectable operation time period (t_p) of TPL5100 timer; 16, 32, and 64s. From Fig. 2, the series type rectifier exhibits the highest average conversion efficiency with the optimal capacitance. Regarding the timer operation time periods and capacitance value, the use of long time periods, which requires larger capacitance to maximize the efficiency, reduces the power consumption of the oscillator. However, the use of larger capacitor causes a higher leakage current loss. Therefore, this research adopted t_p of $16\,\mathrm{s}$ and a $2\,\mathrm{mF}$ capacitor to minimize capacitor leakage loss.

TABLE I
Rectifier performance comparison

Topology	No. of diodes	Peak eff (%)	Avg eff (%)	Open voltage (V)
Series	1	21.9	17.3	0.21
One	2	16.7	13.3	0.29
Two	4	10.2	8.2	0.35

$$I = \frac{V}{Z} = C\frac{dV}{dt} = C\frac{dV}{dZ}\frac{dZ}{dt} \qquad \frac{dZ}{dt} = \frac{V(t)}{Z(t)}\frac{1}{C\frac{dV}{dZ}(Z(t))} \quad (1)$$

$$V = \frac{p_1 Z + p_2}{Z + q_1} \qquad \frac{dV}{dZ} = \frac{p_1 q_1 - p_2}{(Z + q_1)^2} \quad (2)$$

Based on the analysis, a series type rectifier was fabricated as depicted in Fig. 3(a). For this prototype, S_L, S_P, and S_A are $17.6\,\mathrm{mm}$, $13.2\,\mathrm{mm}$, and $80.3°$, respectively. Fig. 3 (b) shows simulated and measured output voltage with respect to load resistance, and the curve fitting from the measurement is also

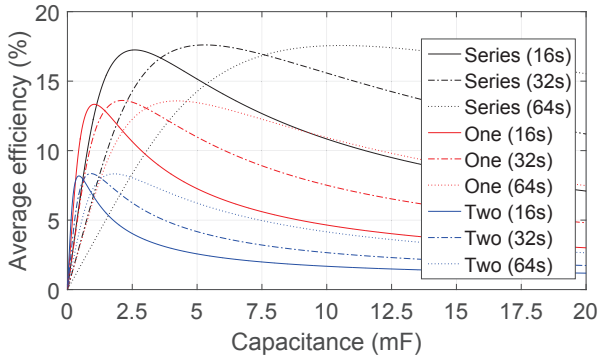

Fig. 2. Comparison of average RF-dc conversion efficiency with respect to the charge tank capacitance values and different timer operation periods with a series rectifier, a one-, and a two-stage voltage multiplier.

depicted, and they have a good agreement. Fig. 3 (c) is the measured and estimated 2 mF capacitor voltage with at each time while charging with the fabricated rectifier prototype with −20 dBm RF input power. The measurement and estimation exhibits a good agreement proving the accuracy of the estimation model. The peak and average RF-dc conversion efficiency are 24.0 % and 17.6 % with 2 mF capacitor and t_p of 16 s from the measurements of the rectifier prototype.

III. DC-DC Conversion Circuit Design and Characterization

Since the output voltage from the rectifier is too low to directly drive practical ICs, a dc-dc boost converter circuit is required. From preliminary measurements, the TPL5100 timer requires 1.5 V, which is the highest required voltage in the system, to start the operation. Therefore, the goal of this study is to generate more than 1.5 V from a dc-dc converter. Fig. 4 shows a typical dc-dc converter circuit topology, which is composed of a charge tank capacitor (C_t), an inductor (L), an N-MOSFET (Q_1), a Schottky diode (D_1), and an output capacitor (C_{out}). The gate terminal of the FET is triggered by the TS3001 oscillator. The selection of each component and of the oscillation frequency is very important to maximize dc-dc conversion efficiency. The aggregated power loss (P_{loss}) in the circuit is the summation of the control (P_{ctrl}), conduction (P_{cond}), and switching (P_{sw}) losses [9]. Therefore, $P_{av} = P_{RFdc} - P_{loss}$ where P_{av} is available power from the system and P_{RFdc} is the average power of the RF-dc conversion circuit. The control loss, which is the minimum required power to operate the system, is associated with the power consumption of the timer and the oscillator ICs. To minimize the oscillator power consumption without degrading the performance of the dc-dc converter, the operation frequency was selected to be 10 kHz [9]. Table II summarizes measured current consumption and operation time of each IC with in t_p of 16 s. TPL5100 timer IC has the fixed MOSFET switch drive time of 31.25 ms which limits the operation time of the oscillator. However, a decoupling capacitor (C_d) connected to the Vdd of the oscillator circuit can extends the operation time of the oscillator. With the datasheet recommended value of 0.1 µF sustain the operation of the oscillator for extra 30 ms

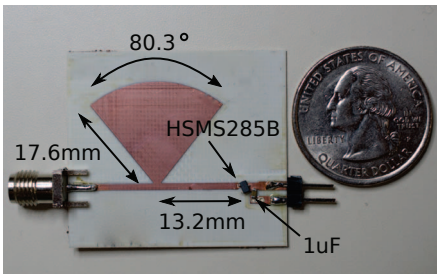

(a)

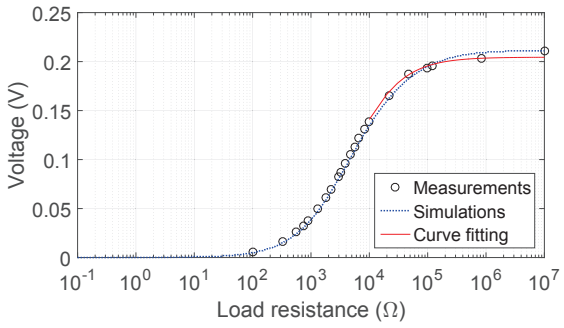

(b)

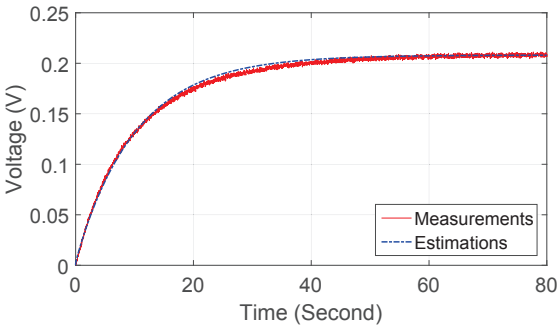

(c)

Fig. 3. (a) Series rectifier prototype. (b) Measured, simulated, and curve fitted output voltage of the recfier with a varied load resistance. (c) Measured and estimated 2 mF capacitor voltage while charging with respect to time.

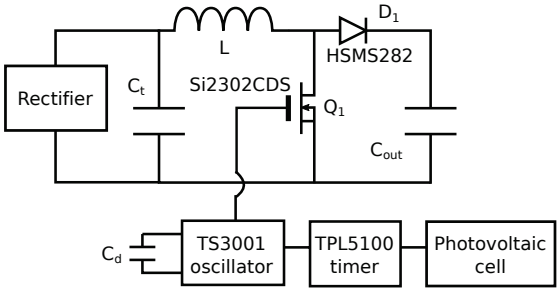

Fig. 4. Circuit schematic of a dc-dc boost converter.

making the total operation time to be about 60 ms with 1.5 V input voltage. The minimum P_{ctrl} is 59 nW, which is an ultra low value that is another goal that needs to be achieved to realize positive available power. Regarding other components, Avago HSMS282 Schottky diode, Vishay Si2302CDS N-MOSFET, and Murata 19R104C (100 µF) inductor were chosen to minimize P_{cond} and P_{sw}.

TABLE II
COMPONENTS OF DC-DC CONVERTER

Component	Part no.	Operation time	Current
Timer	TPL5100	Continuous (31.25 ms MOSFET drive time)	32.6 nA @1.5 V 36.4 nA @1.8 V
Oscillator	TS3001	60 ms @1.5 V	1.34 µA @1.0 V 1.8 µA @1.5 V 2.4 µA @1.8 V

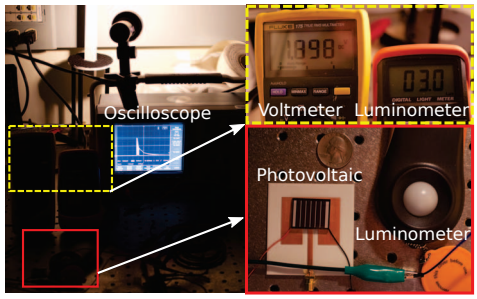

(a)

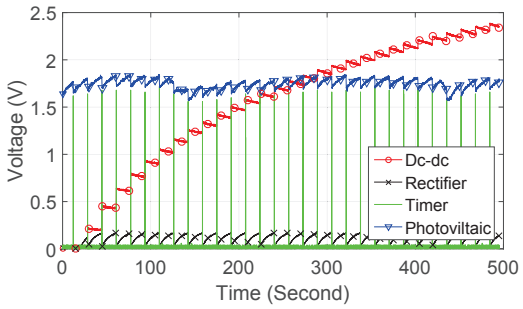

(b)

Fig. 5. (a) Operation test of the dc-dc converter prototype in a darkroom. (b) Measured output voltage from the dc-dc converter, the rectifier, the timer, and the PV during operation test.

IV. Selection of PV Cell and Operation Test

Since the control system requires only 59 nW of power to operate, the output voltage, instead of the output power, under low light irradiation is a key factor of the selection of a PV cell. Therefore, Panasonic AM-5610CAR 25 mm by 20 mm amorphous silicon solar cell which exhibits 5.1 V open voltage under 1 sun irradiation was selected. As depicted in Fig. 5 (b) the PV cell, which can be mounted on a 2.4 GHz patch antenna, exhibits 1.9 V of open voltage which supports the operation of the system under 3 lx = 440 nW · cm^{-2} irradiation, which is 10^2 and 10^4 times weaker than office lighting and direct sunlight, respectively. 3.4 lx is dark limit of civil twilight under a clear sky, so 3 lx light irradiation is considered as night time. Fig. 5 (c) shows the output voltage from the dc-dc converter, the rectifier, the timer, and the PV cell during operation under these darkroom irradiation conditions for −20 dBm ambient RF input power. The dc-dc converter successfully charges 100 µF capacitor to more than 2.4 V within 450 s with the dc-dc conversion efficiency of 38 % and the maximum output voltage reaches to 3 V. The average system output power is 643 nW which is 10.9 times higher than the minimum required system power.

V. Conclusion

In this paper, the design process of a novel fully autonomous ultra-low power hybrid RF/PV energy harvesting system was discussed. Based on the simulated and the measured relationship between the output voltage of the rectifier and the load resistance value, the optimal rectifier topology and the charge tank capacitor value were analytically determined. The rectifier exhibited the peak and average RF-dc conversion efficiency value of 24.0 % and 17.6 % for a 2 mF capacitor and t_p of 16 s from the measurements. Similarly, the PV powered dc-dc converter circuit which requires a minimum of 59 nW and operates effectively even under the extremely low light irradiation of 3 lx was designed and capable to successfully charge the output capacitor, and the net positive output power with output voltage of 1.5 V was confirmed from -25.0 dBm of RF input power which is 4 dB and 9.4 dB lower than state-of-the-art autonomous RF energy harvester [2] and hybrid RF/solar energy harvester [10], respectively. This can be applied for such as autonomous indoor structural health monitoring.

VI. Acknowledgment

The work of J. Bito, J. G. Hester and M. M. Tentzeris was supported by National Science Foundation (NSF), Defense Threat Reduction Agency (DTRA), and Texas Instruments.

References

[1] S. Kim, R. Vyas, J. Bito, K. Niotaki, A. Collado, A. Georgiadis, and M. Tentzeris, "Ambient RF Energy-Harvesting Technologies for Self-Sustainable Standalone Wireless Sensor Platforms," *Proc. IEEE*, vol. 102, no. 11, pp. 1649–1666, Nov. 2014.

[2] K. Gudan, S. Shao, J. J. Hull, A. Hoang, J. Ensworth, and M. S. Reynolds, "Ultra-low power autonomous 2.4GHz RF energy harvesting and storage system," in *2015 IEEE Int. Conf. on RFID-TA*, Tokyo, Japan, Sep 2015.

[3] K. Niotaki, F. Giuppi, A. Georgiadis, and A. Collado, "Solar/EM energy harvester for autonomous operation of a monitoring sensor platform," *Wireless Power Transfer*, vol. 1, no. 01, pp. 44–50, Mar 2014.

[4] Y. Zhou, T. M. Khan, J. W. Shim, A. Dindar, C. Fuentes-Hernandez, and B. Kippelen, "All-plastic solar cells with a high photovoltaic dynamic range," *J. of Materials Chemistry A*, vol. 2, no. 10, p. 3492, 2014.

[5] J. Tong, S. Xiong, Y. Zhou, L. Mao, X. Min, Z. Li, F. Jiang, W. Meng, F. Qin, T. Liu, and et al., "Flexible all-solution-processed all-plastic multijunction solar cells for powering electronic devices," *Mater. Horiz.*, vol. 3, no. 5, pp. 452–459, 2016.

[6] S. A. Nauroze, J. G. Hester, B. K. Tehrani, W. Su, J. Bito, R. Bahr, J. Kimionis, and M. M. Tentzeris, "Additively manufactured RF components and modules: Toward empowering the birth of cost-efficient dense and ubiquitous iot implementations," *Proc. IEEE*, pp. 1–21, 2017.

[7] J. G. Hester, S. Kim, J. Bito, T. Le, J. Kimionis, D. Revier, C. Saintsing, S. Wenjing, B. Tehrani, A. Traille, B. S. Cook, and M. M. Tentzeris, "Additively Manufactured Nanotechnology and Origami-Enabled Flexible Microwave Electronics," *Proc. IEEE*, vol. 103, no. 4, pp. 583–606, Apr. 2015.

[8] J. Bito, B. Tehrani, B. Cook, and M. Tentzeris, "Fully inkjet-printed multilayer microstrip patch antenna for Ku-band applications," in *2014 IEEE Antennas and Propag. Society Int. Symp.*, Memphis, TN, USA, July. 2014, pp. 854–855.

[9] T. Paing, J. Shin, R. Zane, and Z. Popovic, "Resistor Emulation Approach to Low-Power RF Energy Harvesting," *IEEE Trans. Power Electron.*, vol. 23, no. 3, pp. 1494–1501, May 2008.

[10] J. Bito, R. Bahr, J. G. Hester, S. A. Nauroze, A. Georgiadis, and M. M. Tentzeris, "A Novel Solar and Electromagnetic Energy Harvesting System With a 3-D Printed Package for Energy Efficient Internet-of-Things Wireless Sensors," *IEEE Trans. Microw. Theory Techn.*, vol. PP, pp. 1–12, 2017.